Catalytic mechanism and protein engineering of copper-containing nitrite reductase

Wijma, Hein Jakob

Chapter 5

Catalytic Cycle of Copper-Containing Nitrite Reductase, Reversible Inactivation and Irreversible Reduction

This chapter is to be submitted.

Abstract

In copper-containing nitrite reductase, a type-1 copper site receives an electron from a physiological donor. The electron is subsequently transferred to the type-2 active site, where nitrite is reduced to nitric oxide. The reduced type-2 copper undergoes a conformational change after which it can no longer bind the nitrite substrate. It is found here that this isomerization is very slow compared to the turn-over rate of the enzyme, and reversible. Therefore, a catalytic cycle in which the reduced type-2 site binds nitrite is possible. Still, the inactive reduced state is relevant, during steady-state catalytic turn-over approximately half the nitrite reductase molecules are in this temporarily inactive state. Furthermore, at saturating nitrite concentrations, type-1 to type-2 electron transfer is irreversible. This affirms the conclusion that internal electron transfer is rate-limiting for copper-containing nitrite reductase. The midpoint potential of the type-1 was found to decrease by a 100 mV going from pH 4.5 to pH 8.5, and was not altered by binding of nitrite to the nearby type-2 site.

Introduction

Copper-containing nitrite reductase (NiR) is an important enzyme in denitrifying organisms; in bacteria, archaea and fungi (*56, 59, 129*) it catalyses the one electron reduction of nitrite to nitric oxide

$$NO_2^- + 2H^+ + e^- \rightleftarrows NO + H_2O \quad (1),$$

a step in the denitrification pathway. The enzyme catalyses bidirectionally, the rates of forward and reverse reaction are the same at approximately pH 7.5 (chapter 3). In pathogens, NiR is known to enhance the resistance against human sera in *Neisseria gonorrhoeae* (*62*) and it allows *Neisseria meningitides* to respire on nitrite under the microaerobic conditions encountered during host colonization and disease (*64*). There is also an interest (*65-67*) in applying NiR in amperometric biosensors to monitor nitrite in body fluids, natural streams and waste waters.

NiR is a homotrimer (*77*) in which each subunit contains a type-1 electron transfer site and a type-2 catalytic site (*78, 81*). The type-1 site is near the surface and accepts electrons from the physiological electron donor (*76, 79, 80*), which are then transferred to the buried catalytic type-2 site. The type-2 copper atom is bound by the N_ε atoms of three histidine residues; the fourth coordination position is available for the binding of nitrite (*131*). Two other conserved residues in the active site, an aspartate and a histidine, are needed for efficient catalysis (*83-86*). During the catalytic cycle, nitrite binding and type-2 site reduction may occur in random order (step 1 to 4 in scheme 1). The steady-state rate of reduction is given by (chapter 4)

$$k_t = k_{cat}{}^A[NO_2^-]\left(\frac{1+\frac{k_{cat}{}^B}{k_{cat}{}^A}\frac{[NO_2^-]}{K_M{}^B}}{K_M{}^A+[NO_2^-]+\frac{[NO_2^-]^2}{K_M{}^B}}\right) \quad (2),$$

in which k_t is the turn-over rate of the NiR, and $K_M{}^A$ and $K_M{}^B$ are the Michaelis constants for the lower and upper route in scheme 1, respectively. The $k_{cat}{}^A$ and $k_{cat}{}^B$ are the rate constants for the lower and upper route (chapter 4). Below pH 6.5 there is substrate inhibition ($k_{cat}{}^B/k_{cat}{}^A < 1$). Elsewhere (chapter 4) we presented evidence for the random order of the steps in the catalytic mechanism (nitrite binding and type-2 site reduction, scheme 1, steps 1 - 4), but not for the occurrence of an inactive reduced state (IRS, see scheme 1 step 5), that does not bind nitrite (*54*).

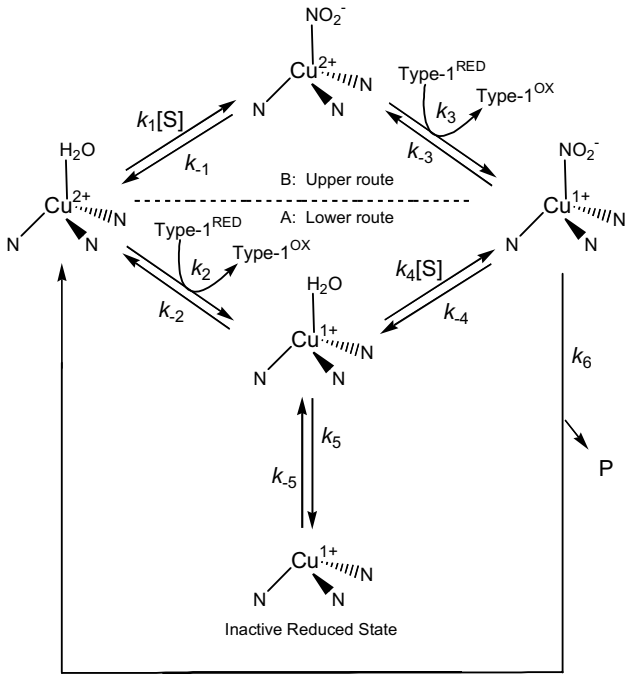

Scheme 1: Proposed catalytic cycle of NiR.
The nitrite is depicted as deprotonated but it may also be protonated in the catalytic cycle. The type-2 Cu atom is depicted with the N_ε atoms of the ligating histidines.

An attractive method to study redox-active enzymes is protein-film voltammetry (*123, 164, 180*), in which a film of enzyme molecules is immobilized on an electrode. The current through the electrode reports on the catalytic activity of the immobilized redox enzyme, which can be studied as a function of electrode potential, substrate concentration, and time. By this method we show that there is a slow isomerization between an IRS and a 'normal' reduced type-2 site. Furthermore, we find that at saturating nitrite concentrations the type-1→type-2 electron transfer is rate-limiting and that the midpoint potential of the type-1 site is not altered by the binding of nitrite to the nearby type-2 site.

Materials and Methods

General

Wild-type NiR was prepared as described (chapter 3) with omission of the gel-filtration step. We found that the gel-filtration step did not improve the response on the electrode. All experiments were carried out with a pyrolytic graphite edge (PGE) electrode on which NiR was immobilized as described previously (chapter 4).The kinetic constants K_M^A, K_M^B and k_{cat}^B/k_{cat}^A were determined as described in chapter 4. Potentiometric titrations were carried out as described in chapter 7. Nitric oxide gas (0.5 % NO in 99.5 % N_2) was scrubbed with 1 M KOH and 0.1 M potassium phosphate pH 7 prior to application. Bubbling with this gas-mixture gives a 16 µM nitric oxide solution at 1°C (*152*). Unless mentioned otherwise, all experiments were carried out at 1 ± 1 °C. At all nitrite concentrations faster rotation did not increase the current.

Pre Steady-State Kinetics

When in the catalytic cycle (scheme 1), k_5 and k_{-5} are much slower than the other steps, then k_t (the catalytic turn-over rate) will change exponentially with time to reach its steady-state value (see supplementary material). When the assay is started with oxidized enzyme, k_t will decrease in time (the assay starts with 100 % active enzyme and part of it ends up in the IRS), but when the assay is started with reduced enzyme (where there is an equilibrium between active reduced enzyme and enzyme in the IRS), k_t will increase in time (the nitrite pulls enzyme out of the IRS). It can be derived (*179*) that the rate of activation (k_{act}) and inactivation (k_{inact}) are identical (*181*) and depend on nitrite concentration according to

$$k_{act} = k_{inact} = k_{-5} + k_5\left(\frac{1 + K_A[NO_2^-]}{1 + K_B[NO_2^-] + K_C[NO_2^-]^2}\right), \text{ with} \quad (3)$$

$$K_A \equiv \frac{k_1 k_3 k_{-4}}{k_2(k_7 + k_{-4})(k_{-1} + k_3)}, \quad (3A)$$

$$K_B \equiv \frac{k_1 k_3 k_{-4} + k_4 k_{-1} k_7 + k_4 k_3 k_7 + k_4 k_2 k_{-1} + k_4 k_2 k_3}{k_2(k_7 + k_{-4})(k_{-1} + k_3)}, \text{ and} \quad (3B)$$

$$K_C \equiv \frac{k_1 k_4 (k_7 + k_3)}{k_2(k_{-1} + k_3)(k_7 + k_{-4})} \quad (3C).$$

Equation 3 contains too many parameters to fit the data reliably, but it does show that when the nitrite concentration approaches zero, $k_{act} = k_{-5} + k_5$, while at very high nitrite concentration, $k_{act} = k_{-5}$.

Potential dependence of current

The dependence of enzymatic current (i) on electrode potential can yield information on the reduction potential of the active site and/or that of its electron relay centers. The simplest model (*164*) to analyze the dependence of NiRs enzymatic current on electrode potential would be one in which electron transfer between electrode and type-2 active site is fast compared to the turn-over rate of the enzyme k_t (, which implies that the enzyme that the enzyme is optimally oriented for electron transfer with the electrode). Within this limit, the depletion of electrons from the type-2 site via k_t is too slow to disturb the redox-equilibrium between electrode and the type-2 site. Then, because i is proportional to the fraction of reduced type-2 sites, the catalytic current depends on the electrode potential according to the Nernst equation (Figure 1A). The first derivative (Figure 1B) of this catalytic voltammogram shows a single symmetrical peak with a maximum at the position of the midpoint potential (E_M) of the active site. Notice that, when the electron transfer between type-1 and type-2 site is slow, the observed midpoint potential will be that of the type-1 site, since k_t now depends on the fraction of reduced type-1 site. The limiting current (i_{lim}) in Figure 1B corresponds to 100 % reduced type-2 (or 100 % reduced type-1 site). This i_{lim} is proportional (*164*) to k_t via

$$i_{lim} = k_t F A \Gamma \qquad (4),$$

in which F is Faraday's constant, A is the surface area of the electrode, and Γ is the surface coverage expressed in enzyme molecules per unit area.

In a more realistic model (*182*), part of the immobilized NiRs are not optimally oriented for electron transfer with the electrode. For those NiRs electron transfer between electrode and type-1 site (the electron entry point) is rate-limiting. This can be modeled (*182*) with three extra parameters, a range of distances (d_R) between electrode and redox centre times the decay constant β for electron transfer (βd_R in equation 5) and the rate of electron transfer when the enzyme is optimally oriented for electron transfer to the electrode (k_0^{max}). With an even distribution of enzyme molecules over d_R, the model predicts (*182*) a linear increase in current with increasing driving force (Figure 1C). This is indeed found for most immobilized enzymes (*182*). In the derivative of the catalytic voltammogram (Figure 1D), a peak still occurs at the midpoint potential, unless k_t/k_0^{max} is so low that that the peak becomes negligible compared to the subsequent linear increase in current versus electrode potential.

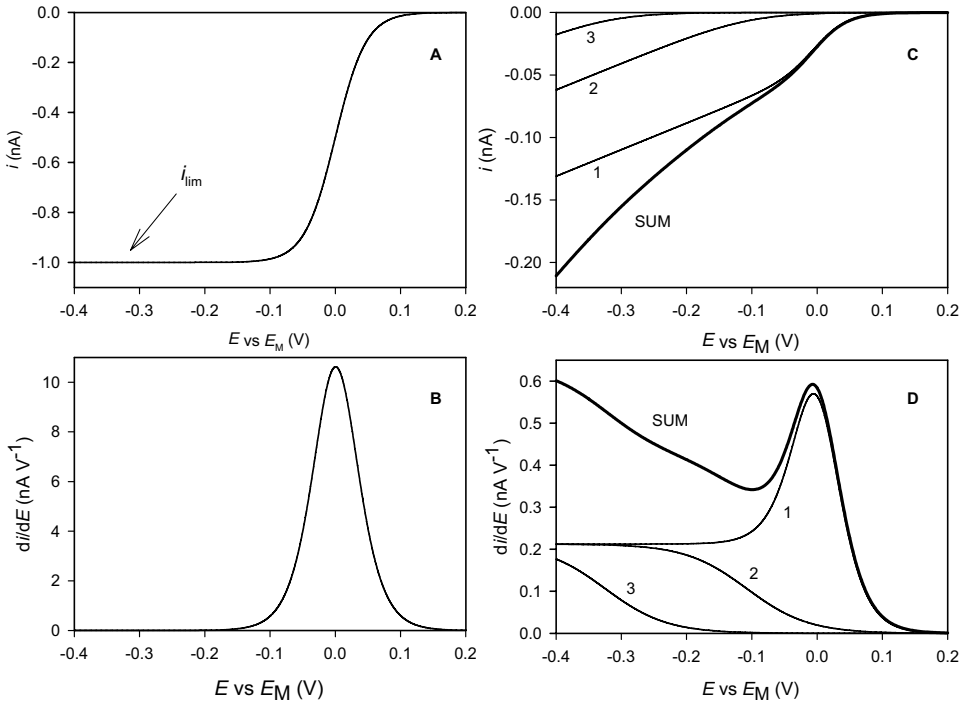

Figure 1: Effect of heterogeneity on catalytic voltammograms for a one-electron reductase

The value of i_{lim} is chosen as 1 nA reductive current and E_M = 0 mV for all plots. (A) If electron transfer with the electrode and electron transfer within the enzyme is fast, the catalytic current is determined by k_t and E_M of the type-2 site according to the Nernst equation. The resulting shape of the catalytic response is shown (B) First derivative of the curve in panel A. (C) i versus E curves calculated assuming that distances of the redox-site to the electrode are distributed over a range d_R and a k_0^{max} is the rate of electron transfer to the enzymes that are closest to the electrode. For a trimeric enzyme there are three sets of k_t/k_0^{max} (labeled A, B, and C) while d_R is assumed to be identical in value for each monomer, $k_t/k_0^{max\_A}$ (plot 1) is 0.01, $k_t/k_0^{max\_B}$ (plot 2) is 10, $k_t/k_0^{max\_C}$ (plot 3) is 1000, and βd_R = 100. (D) First derivatives of the curves in panel C.

Equation 5 describes the dependence of catalytic current on electrode potential (E) for a one electron reductase that displays the discussed heterogeneity in orientations on the electrode.

$$i = \frac{i_{\lim}}{\beta d_R}\,\mathrm{u}\,\frac{1}{1+\mathrm{v}^2} \qquad \text{, with} \tag{5}$$

$$\mathrm{u} \equiv \ln\left(\left(1+\mathrm{v}^2+\frac{k_t}{k_0^{\max}}\mathrm{v}\right)\Big/\frac{k_t}{k_0^{\max}}\mathrm{v}\right) \qquad \text{, and} \tag{5a}$$

$$\mathrm{v} \equiv \exp\left[\frac{F}{2R\mathrm{T}}\left(E-E_M\right)\right] \tag{5b}$$

The fit parameters in equation 5 are E_M, $i_{lim}/\beta d_R$, and k_t/k_0^{max}. Information about $i_{lim}/\beta d_R$ is stored in the slope while the initial curvature reports on k_t/k_0^{max} and E_M. For the trimeric NiR, we found that the voltammograms are consistent with three populations of active sites (close to the electrode, further away, and furthest away, see Figure 1C and 1D). The data were fitted to a single E_M and $i_{lim}/\beta d_R$, and three values of k_t/k_0^{max}, $k_t/k_0^{max\_A}$, $k_t/k_0^{max\_B}$, $k_t/k_0^{max\_C}$, corresponding with the different monomers. The data were fitted with

$$\frac{di}{dE} = -\frac{i_{\lim}}{\beta d_R}\,\frac{F}{2R\mathrm{T}}\,\frac{1+2\mathrm{u}\left(\mathrm{v}^2+\mathrm{v}^4+\frac{k_t}{k_0^{\max}}\mathrm{v}^3\right)-\mathrm{v}^4}{\left(1+\mathrm{v}^2+\frac{k_t}{k_0^{\max}}\mathrm{v}\right)\left(1+\mathrm{v}^2\right)^2} \tag{6},$$

the first derivative of equation 5; in the derivative voltammogram E_M is far more obvious (compare the SUM trace in panel C and D of Figure 1). In equations 5 and 6, R is the gas constant, and T is the absolute temperature. Equation 5 was derived along the same lines as used by Léger (*182*) for a two electron reductase.

Results and Discussion

Reductive inactivation

Nitrite reductase (NiR) was immobilized on a PGE electrode. In the presence of nitrite, catalytic currents were observed at electrode potentials below 0.3 V versus NHE (Figure 2A). In the absence of nitrite, no voltammetric features were present that could be assigned to the type-1/type-2 site of NiR, which suggests that the surface coverage by the enzyme is too low (< 3 pmol cm^{-2} (*174*)) for a signal to be detectable. From equation 4, with a k_t of 10^3 s^{-1} (chapter 3) and a i_{lim} of 500 nA (Figure 2A), a surface coverage of ≈ 0.1 pmol cm^{-2} is calculated which is low, indeed.

When starting at oxidizing potential, the current observed on the forward scan was always higher than on the return scan (Figure 2B). When starting at reducing potential, the return scan had significant more amplitude (results not shown). Furthermore, when the scan rate was reduced starting at oxidizing potential, the catalytic current diminished (Figure 2B). These observations can be explained by assuming that a slow reductive inactivation occurs. To investigate this further, chronoamperometry was used.

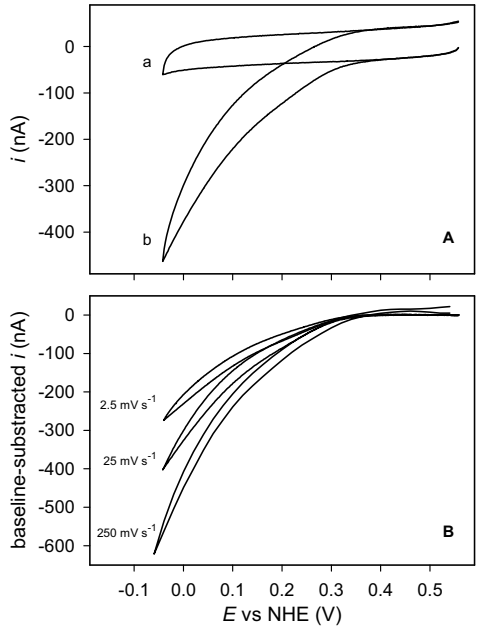

Figure 2: Effect of scan rate on catalytic amplitude.
(A) Cyclic voltammogram in the absence (a) and presence (b) of nitrite (1 mM), scan rate 25 mV s^{-1}. (B) Baseline subtracted current (b-a) at different scan rates. The NiR painted PGE electrode was rotated at 3000 rpm in malate/MES/HEPES buffer (25 mM of each component, 1 °C, pH 6.7).

The reductive inactivation was measured by first pre-treating the electrode at oxidizing potential (560 mV versus NHE, 100 s) to ensure that all enzyme was in the active state. Then, after starting the assay by lowering the potential to 60 mV versus NHE, a decrease in current over time was observed, also in the absence of nitrite (Figure 3A). This latter a-specific current was reproducible enough to be subtracted (see traces labeled A in Figure 3B for the difference between consecutive traces). After subtraction of the a-specific current it showed (Figure 3B) that indeed a slow decrease in the catalytic current occurred, which could be fitted with a single exponential (rate: $k_{obs} \approx 0.2\ s^{-1}$). The magnitude of the decrease ($i(0)$-$i(\infty)$) and the steady-state current ($i(\infty)$) could be fit (Figure 3C) with equation 2 resulting in similar values K_M^A, K_M^B and k_{cat}^B/k_{cat}^A (Table 1), confirming that both $i(\infty)$ and ($i(0)$-$i(\infty)$) reflect the activity of NiR. Assuming scheme 1 it is expected that, equation 2 also obtains when no IRS has formed yet (chapter 4) and that the formation of the IRS influences the catalytic constants, indeed.

A plot of k_{obs} versus nitrite concentration (Figure 3D) shows that lower rates are observed at higher nitrite concentration. This agrees with what is expected from scheme 1, where a single inactive state equilibrates with a reduced active state that is able to bind nitrite. As remarked before, when the nitrite concentration approaches zero, $k_{obs} = k_5 + k_{-5}$, while at high nitrite concentrations, $k_{obs} = k_{-5}$. Thus, at pH 5.3, $k_5 + k_{-5} \approx 0.2\ s^{-1}$, and $k_{-5} \approx 0.1\ s^{-1}$ (Figure 3D).

We also investigated the *activation of pre-reduced* NiR by the addition of nitrite. First the steady state current was measured as a function of nitrite concentration (Figure 4A). It shows a maximum around 300 μM (see arrow 1 in Figure 4A). In the next experiment the electrode was first poised at a reducing potential after which 320 μM of nitrite was added to the solution (see Figure 4B at arrow 1). The current was seen to increase stepwise. This was followed by an exponential phase, with a k_{obs} of $0.2\ s^{-1}$, which we ascribe to slow activation of the inactive form of the enzyme. It might be argued that the time dependent phenomena might in part be related to the time it takes for the nitrite to diffuse to the electrode. Therefore a second addition of nitrite was made producing a solution concentration of 3200 μM of nitrite. From Figure 4A it is clear that at this concentration (arrow 2) addition of nitrite results in substrate inhibition. Decrease of activity is indeed seen in the time trace of Figure 4B (arrow 2) and the change in current is a step function, meaning that on the time scale of Figure 4B diffusion is instantaneous.

The data in Figure 4B (arrow 1) indicate that, in the absence of nitrite, there are approximately equal amounts of reduced NiR with active and inactive type-2 sites (thus $k_5 \approx k_{-5}$). The rates of inactivation and activation are equal and do not depend on the electrode potential from -200 to +100 mV versus NHE (Figure 5), in agreement with scheme 1.

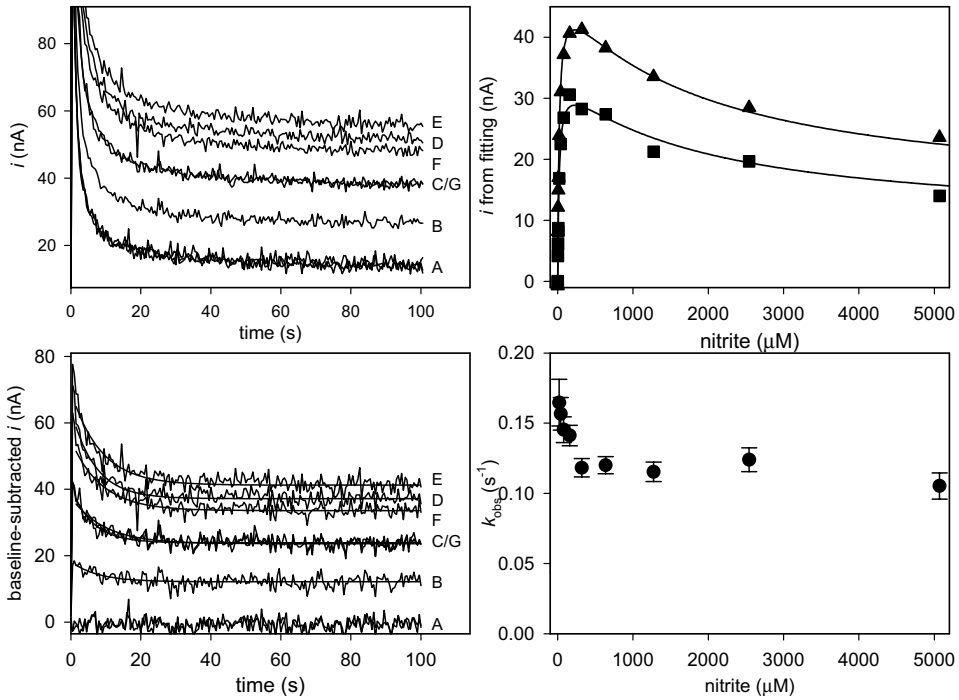

Figure 3: Chronoamperometry of nitrite reductase.
(A) Traces measured for different concentrations of nitrite: A, 0 μM (3 traces); B, 5 μM; C, 20 μM; D, 80 μM; E, 318 μM; F, 1.7 mM; G: 5.07 mM. (B) Baseline subtracted curves fitted to a single exponential [i(t) = i(∞) + [i(0)-i(∞)]exp(-k_{obs}t)]. The first second after the start of the assay was not used for the fit. (C) Plot of the parameters fitted from panel B as a function of nitrite concentration. Triangles, i(∞); squares i(0)-i(∞); lines, group fit. (D) k_{obs} versus nitrite concentration. Observed rates below 20 μM nitrite were omitted as the errors were excessively large. For all panels the conditions were as in Figure 2 except that the pH was 5.3. The electrode was pre-treated at 560 mV versus NHE for 100 seconds, the measurement was started when the potential was switched to 60 mV versus NHE.

Table 1: Kinetic constants obtained from fitting

	K_M^A (μM)	K_M^B (μM)	k_{cat}^B/k_{cat}^A
Figure 3C:			
group fit	20 ± 2	(1.8 ± 0.5) × 10^3	0.3 ± 0.1
i(∞)	16 ± 1	(2.4 ± 0.8) × 10^3	0.3 ± 0.1
i(0)-i(∞)	27 ± 3	(1.1 ± 0.3) × 10^3	0.3 ± 0.1
Effect glycerol:			
without glycerol [A]	40 ± 3	(2.4 ± 0.6) × 10^3	0.3 ± 0.1
with glycerol [B]	61 ± 2	(3.6 ± 0.5) × 10^3	0.32 ± 0.03

[A] pH 5.95, [B] pH 6.05

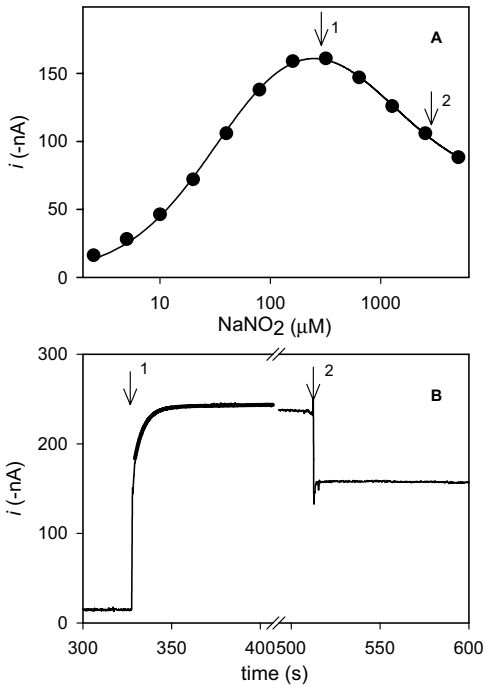

Figure 4: Reactivation of NiR on a rotating disk electrode
(A) Semi-logarithmic plot of steady-state current versus nitrite concentration (pH 5.6). The solid line is a fit to equation 2 (the catalytic current is proportional to k_t in equation 2) yielding i_t^A = -2.1 10^{-8} A, K_M^A = 36 μM, K_M^B= 1.0 mM, and k_{cat}^B/k_{cat}^A = 0.3. (B) Catalytic current as a function of time. At t = 325 s nitrite was added to a concentration of 320 μM (arrow 1). At t = 510 s a second stepwise addition of nitrite was effected (arrow 2, end concentration 3200 μM). The small initial current is the background (corrected for in panel A). The exponential fit is indicated with a thick line. The experiments in panel A and B were done on different enzyme films (resulting in slightly different amplitudes). The RDE was operating at 4000 rpm.

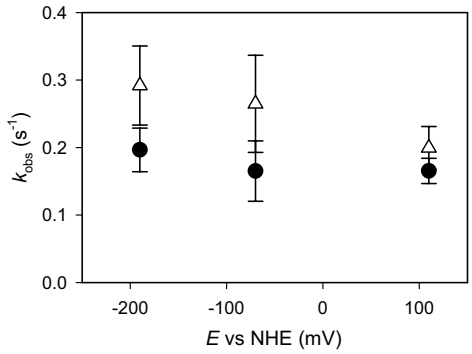

Figure 5: Observed rates of inactivation and reactivation versus electrode potential.
Rate constants obtained from exponential fits (Figure 3 and 4) for activation (filled circles) and inactivation (open triangles) at pH 5.6. The activation was carried out by addition of 320 μM of nitrite while the inactivation was carried out by a voltage step at 3200 μM nitrite.

Dependence of catalytic activity on electrode potential and nitrite concentration

The catalytic voltammograms were further investigated to obtain information about the catalytic cycle of the NiR and about the electron transfer rates between electrode and immobilized NiR. The scan rates (1 - 2.5 mV s^{-1}) were slow enough to ensure equilibrium between active and inactive forms of the reduced NiR (as shown by the semi-reversible traces in Figure 6A and Figure 7). Slower scan rates resulted in a loss of protein film. A clear increase of catalytic current was observed at potentials that exceeded E_M (Figure 6A). As discussed in the Materials and Methods section, this is indicative for a spread of distances between the electrode and the electron entry point of the enzyme. The derivative curve (Figure 6B, gray line) could be fitted assuming three subpopulations, possibly reflecting the trimeric structure of NiR (see caption of Figure 6 for values).

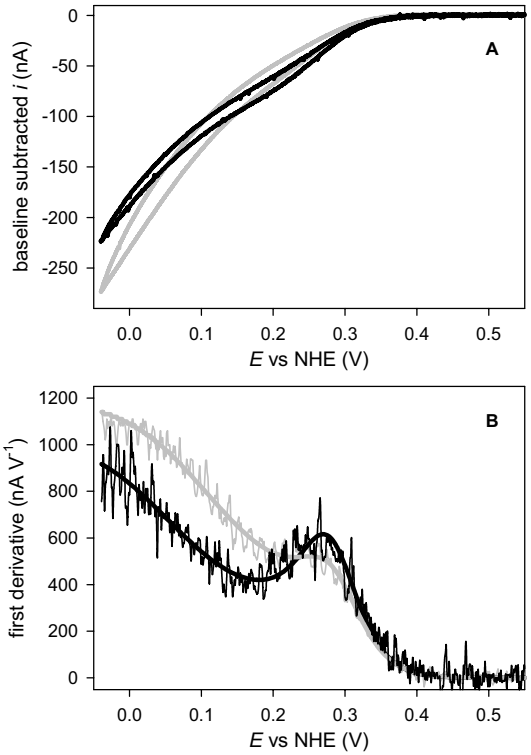

Figure 6: Effect of glycerol on shape of voltammogram
(A) Background subtracted scans at 2.5 mV s^{-1} at pH 6.7, at 1 mM nitrite in the absence of glycerol (gray line) and in the presence of 20% glycerol (black line). (B) First derivatives and fits of these scans with the same color code. The fit to equation 6 produced the following values (the corresponding values in the presence of glycerol are in between parenthesis) E_M = 286 mV versus NHE (281 mV), $k_t/k_0^{max\_A}$ = 0.22 (0.06), $k_t/k_0^{max\_B}$ = 18 (58), $k_t/k_o^{max\_C}$ = 105 (279), $i_{lim}/\beta d_R$ = -18.5nA (-15.9 nA)

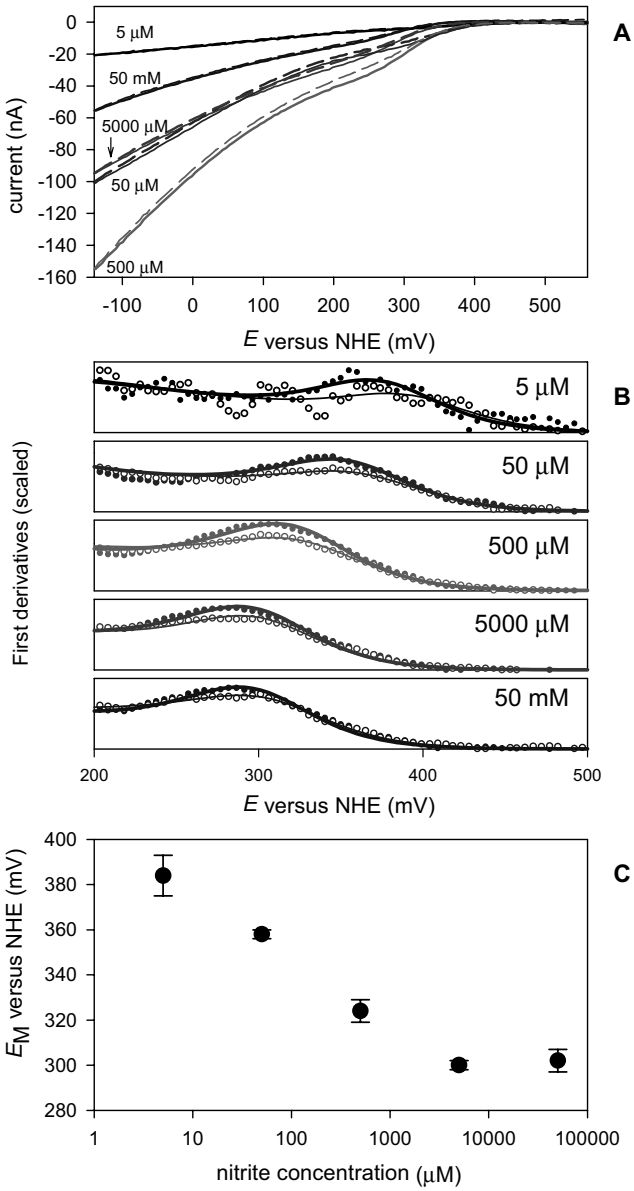

Figure 7: Observed Reduction potential versus nitrite concentration
(A) Background subtracted *i* versus *E* scans at 1 mV s^{-1} at pH 5.6 at nitrite concentrations increasing from 5 μM to 50 mM, see lower panels for color code. Continuous lines denote forward scans, from oxidative to reductive potential, and dashed lines denote backward scans. (B) First derivatives fitted with equation 6. Closed circles are the data from the forward scans and are fitted with a thick line while open circles are the data of the backward scans that are fitted with a thin line. (C) The E_M values obtained from the fitting versus nitrite concentration.

In the presence of 20 % glycerol, the peak that marks the E_M value is more obvious (Figure 6B). From the fitted values of k_t/k_0^{max} for the different subpopulations it appears that glycerol improves the electronic coupling with the nearest subpopulation (see Figure caption). The observed midpoint potential was approximately the same in the presence (281 mV versus NHE) and absence (286 mV versus NHE) of glycerol, as were the K_M^A, K_M^B, and k_{cat}^B/k_{cat}^A (Table 1). Thus, addition of glycerol gave a better accuracy in the determination of E_M while it did not alter the catalytic properties of the enzyme.

The dependence of E_M on nitrite concentration was studied in some detail. A gradual decrease from 385 to 300 mV was observed upon going from 5 μM to 5 mM nitrite (Figure 7), while E_M remained constant beyond 5 mM (up to 50 mM). The simplest explanation for this is that at increasing nitrite concentrations the upper route in scheme 1 prevails (chapter 4) and that with nitrite bound to the type-2 site, the type-1 → type-2 electron transfer (step 3) is much slower than electron exchange of the type-1 site with the electrode. Thus, E_M gradually shifts to the midpoint potential of the type-1 site with increasing $[NO_2^-]$. For the related NiR from *Achromobacter cycloclastes* (82 % identical amino acid sequence) it is indeed found that the type-2 site reduction potential is 50 mV higher than the type-1 site potential at pH 6 (*136*).

Catalytic voltammograms at saturating nitrite concentrations (Figure 8A) were obtained from pH 5 to pH 8.5. From low to high pH the observed E_M (Figure 8B, squares) decreased by 100 mV. The midpoint potentials of the type-1 site versus pH were also determined by potentiometric titration under the same conditions (pH 4 till 9, 20% glycerol, mixed malate-MES-HEPES buffer, temperature 1 °C). Oxidative and reductive titrations gave identical results (Figure 8C). From pH 4.8 till pH 8.8 the midpoint potentials of the type-1 site (Figure 8B, circles with error bars) were identical to the E_M determined in catalytic voltammograms at saturating nitrite concentration. This confirms that at saturating nitrite concentration the type-1→ type-2 electron transfer is rate-limiting and shows that the midpoint potential of the type-1 site is not altered by the nitrite binding to the type-2 site.

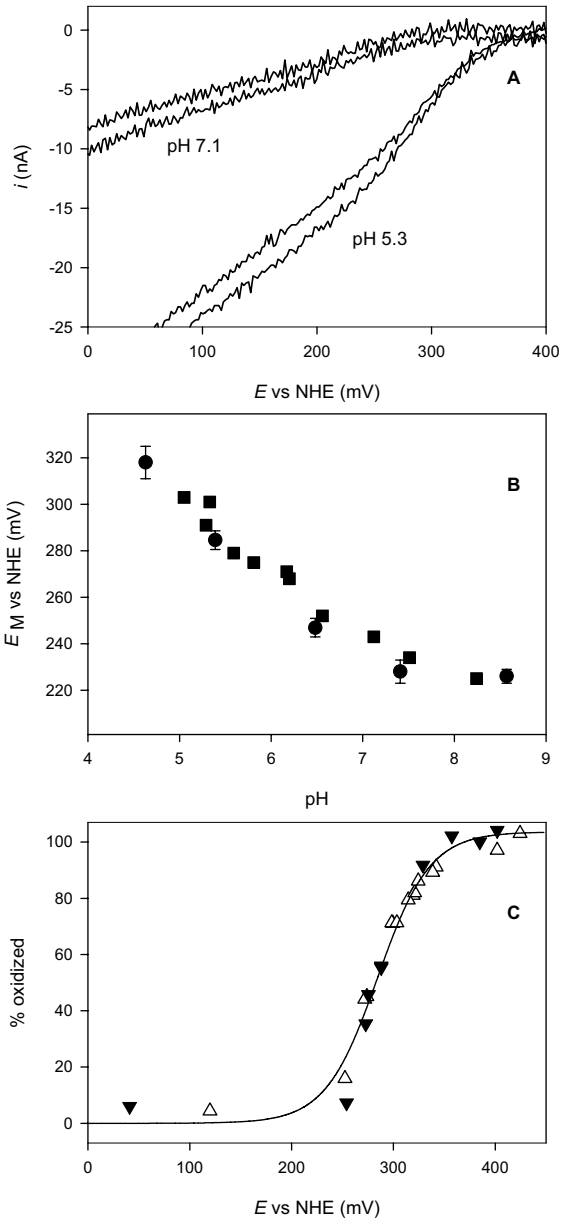

Figure 8: Midpoint potential of the type-1 site versus pH
(A) Background subtracted *i* versus *E* scans (1 mV s^{-1}) at two different pH values (B) Plot of the measured midpoint potentials versus the pH. Squares: observed E_M versus pH at saturating nitrite concentrations (10 mM from pH 5 to 5.6, 50 mM from pH 5.8 to 6.2, 100 mM above pH 6.2) Circles with error bars: the E_M of the type-1 obtained from potentiometric titration. (C) Example of a potentiometric titration (at pH 5.4). The open triangles are of the oxidizing titration, the closed triangles are of the reductive titration. The solid line is a fit of all data to the Nernst equation.

Also with nitric oxide as the substrate catalytic currents could be observed (Figure 9A). At 1° C nitric oxide oxidation is barely detectable at pH 7 (a few nA at 0.6 V versus NHE), increases to a maximum that is stable from pH 8 to 9, and decreases to be no longer detectable at pH 10. Increasing the scan rate from 5 to 25 mV s^{-1} made no difference for the amplitude. We measured the catalytic current on a single protein film for nitrite and for nitric oxide (Figure 9B). The slopes of the catalytic current are equal to $i_{lim} \times F/\beta d_R 2RT$ (equation 6). Therefore the ratio of the slopes equals the catalytic bias on the electrode ($i_{lim}^{forward}/i_{lim}^{reverse} \approx 2$ at pH 6.8, 20 °C, Figure 9B) which is in reasonable agreement with the known catalytic bias ($k_{cat}^{forward}/k_{cat}^{reverse} = 6$, pH 7.0, 25 °C, chapter 3) in solution.

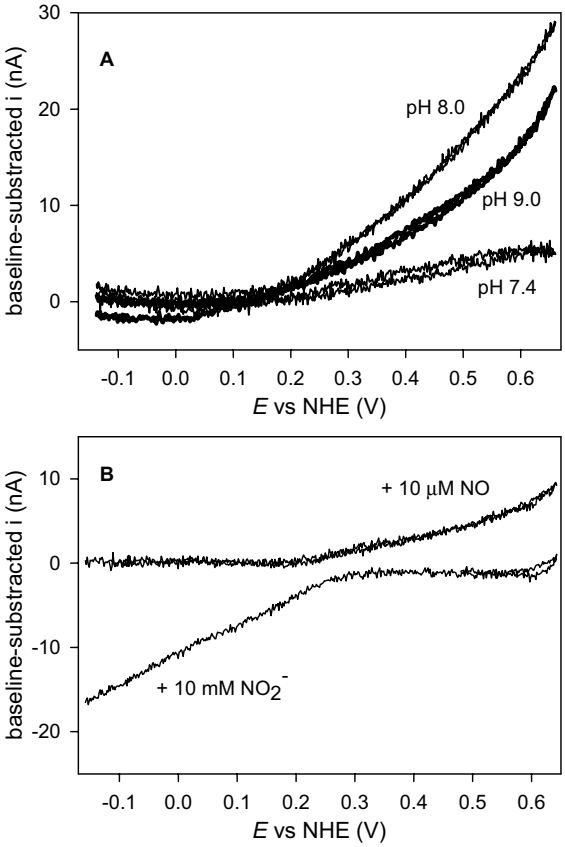

Figure 9: Nitric oxide oxidation by PGE-immobilized NiR
The *i* versus *E* cycles start at reducing potential. (A) Cyclic voltammograms at 1°C and in the presence of 16 μM nitric oxide at a scan rate of 5 mV s^{-1}. Scans are from different protein films; (B) Scans were carried out with a single protein film at 20 °C and pH 6.8, and at a scan rate of 1 mV s^{-1}. The buffer consisted of 25 mM each of the following buffer components: malate, MES, HEPES, TAPS, CHES, and CAPS, and was titrated with NaOH to the desired pH.

Summary and Conclusions

The similar catalytic bias (Figure 9), the similar steady-state kinetics (chapter 4), and the similar restoration of catalytic activity by allosteric effectors in immobilized NiR M150G (results not shown, see chapter 7) indicate that the electrode immobilized NiR has the same catalytic properties as in solution. Earlier it was observed by scanning probe microscopy that NiR, from other organisms, stays intact on the electrode (*33, 183*). The shape of the catalytic voltammograms can be fitted assuming that the trimeric structure of NiR results in slower electron transfer rates from electrode to the redox centers that are further away from the electrode. The near identical values for the E_M obtained from the catalytic voltammograms and the E_M obtained from potentiometric titration (Figure 8B) shows that the modeling is sufficiently accurate to be able to draw conclusions.

Both cyclic voltammograms (Figure 2) and chronoamperometry (Figure 3 - 5) are consistent with scheme 1. The novelty of scheme 1 is that there is an equilibrium between two conformations of the reduced type-2 site, one in which the type-2 site binds nitrite and the IRS in which the type-2 site does not bind nitrite. Earlier it was concluded (*54*) from EXAFS that that the reduced type-2 site was three- instead of four-coordinate and incapable of binding nitrite or other external ligands. The IRS that we observe most likely corresponds to this three-coordinated species (*54*). Figure 2 and 3 show that during catalytic turn-over a significant part of the NiR is inactivated. Most importantly, our data show that the inactivation of active reduced state to IRS is slow and that reactivation of the reduced NiR is possible. This has profound implications for understanding the catalytic cycle and the properties of the reduced type-2 site.

The catalytic voltammograms at saturating nitrite concentration (Figure 7 and 8) are in agreement with an irreversible type-1→ type-2 electron transfer step. This is a corroboration of the conclusion that type-1→ type-2 electron transfer is rate-limiting for NiR (*87, 115, 136*) (chapter 4), a conclusion still based on indirect evidence in the absence of a full kinetic characterization of the catalytic cycle. The identical values in the presence/absence of saturating nitrite concentrations (Figure 8B) indicate that the midpoint potential of the type-1 site is not altered by nitrite binding to the type-2 site.